CHAPTER 2

LITERATURE REVIEW

2.1 Description of Nakornthai Strip Mill

In Thailand the demand of flat products is increasing steadily. Therefore Nakornthai Strip Mill Public Limited is building a steel plant 120 kilometers south-east from Bangkok. The plant is one of the most modern steel plant which is characterized by a very short flexible production line. Several steel grades will be available with short delivering time. The plant is located 35 kilometers from an offshore harbor in Sriracha and will deliver 1.5 million tons of flat steel (with expansion to 3 million tons). NSM combines state of the art processes which are developed or are already applied in the industrial scale such as in North America, Japan and Europe.

2.1.1 Concept of NSM

Today flat steel is produced in the integrated steel plants or mini-mills. The plant of NSM does not belong to one of them. NSM combines advantages of the different principles of steel making. In comparison to the integrated steel

plant, NSM has more advantage in a part of an energy optimization as well as the production line is as short and flexible as the line of a modern mini-mill. Therefore NSM will be one of the first integrated mini-mill in the world.

Due to a combination of the direct reduction unit (Rotary Hearth Furnace process) and the melting unit with integrated scrap preheating, NSM is becoming more independent on scrap (especially for scrap price). The steel plant combined with the Rotary Hearth Furnace is operating economically on a low energy level and environmental friendly. Pre-sorted scrap and sponge iron are charged to the Consteel-Electric Arc Furnace where the material is melted. The liquid steel is then refined in an additional Ladle Heating Furnace and a Vacuum Oxygen Decarburization unit. The secondary metallurgical units require the production of a large variety of different steel grades. This steel is then transported to the Compact Strip Plant which includes a thin slab caster and a hot rolling mill. The steel is cast, solidified, homogenized, descaled, hot rolled and coiled. If required by the customer the steel will be cold rolled, galvanized and tempered [12-14].

2.1.2 Secondary metallurgy

The steel produced in the Consteel-EAF is tapped into a ladle with a capacity of 180 tons that are moved via a transported ferry and a crane to the secondary metallurgy section of the meltshop. This section consists of a 2 ladle heating furnaces and 2 vacuum refining units. The ladles are equipped with 3 large porous plugs and have a freeboard of 1.5 m.

2.1.2.1 Ladle Heating Furnace with integrated deslagging station

NSM uses two LHF with a capacity of 180 tons which are delivered by Mannesmann Demag Huettentechnik (MDH) in Germany. Each furnace requires its energy from a 50 MVA transformer. Alloying elements in the form of lumpy material or wires are charged through openings in the roof of the furnace to the ladle. Three large porous plugs and the 1.5 m. freeboard of the ladle guarantee an optimized mixing of the melt as well as an acceleration of the metallurgical reactions. The skipping machine for deslagging is located near by the furnace which removes a ladle slag after finish of heating and refining performances.

2.1.2.2 Vacuum oxygen decarburization (VOD)

The vacuum oxygen decarburization units, delivered by Mannesmann Demag Huettentechnik/MESSO in Germany are working with vacuum pumps that can adjust a low pressure of 0.5 mbar minimum. Especially in this unit, the porous plugs and the freeboard achieve with the additional low pressure and optimized mixing of the bath as well as quick chemical reactions such as decarburization, desulfurization and degassing (N, H). Openings in the roof allow the addition of alloys with lumpy material and sampling during the process. An installed oxygen lance centered on the furnace roof can penetrate through the opening in the middle of the ladle.

A quick chemical laboratory of the meltshop is located near by the LHFs and VODs where the chemical composition of the steel is determined in a short time.

2.2 Fundamental of secondary metallurgical steel treatment

2.2.1 Desulfurization

Steel desulfurization is mainly driven by metal-slag reactions. The ladle slag is based on $CaO-Al_2O_3-SiO_2$ ternary system [15-18]. In order to obtain optimal desulfurization it is necessary to achieve a lime saturated slag. By careful adjustment of a lime saturated ladle top slag at the beginning of the vacuum treatment, it is possible to obtain more than 95% degree of desulfurization [17,18].

The definition of lime saturation index is the ratio of the actual CaO-content to the saturation CaO-content, when the ratio is equal 1, i.e. the slag is lime saturated slag. If the ratio is greater than 1 the slag is supersaturated, it is undersaturated if ratio lower than 1. Figure 2.1 shows lines of constant lime saturation indices in the $CaO-Al_2O_3-SiO_2$ ternary system [17,19]. The desulfurization potential (the definition is given later) is a function of the saturation degree. The slag shows the highest desulfurization potential when it is a lime saturated slag. In case of an undersaturated slag the decrease in desulfurization is influenced by the decrease of lime activity and increase of alumina activity in the slag. In case of supersaturated slag, the reason of the

decrease in desulfurization efficiency is caused by poor kinetic conditions due to the heterogeneity of the slag.

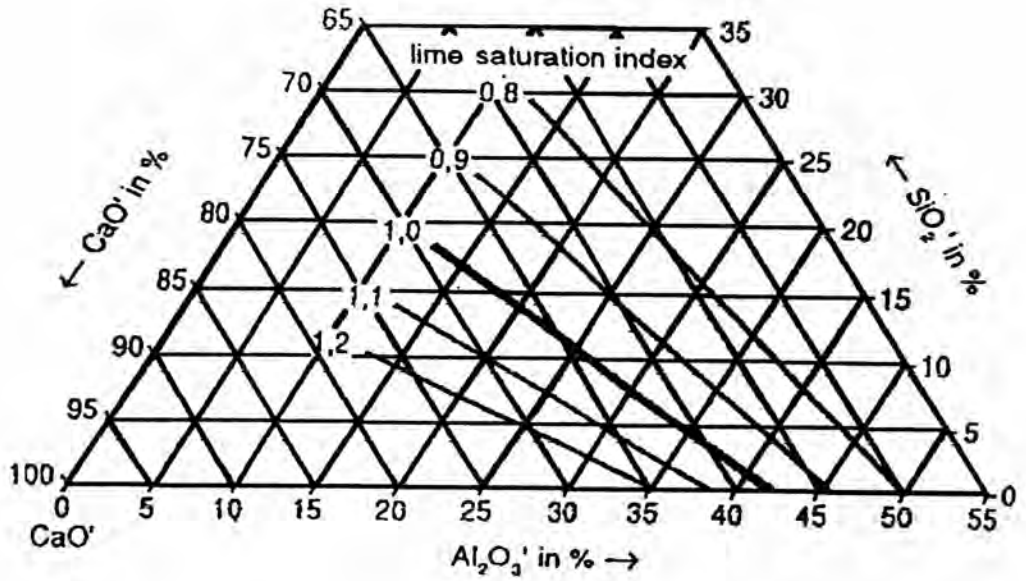

Figure 2.1 Lime saturation index in the system $CaO-Al_2O_3-SiO_2$ [17,19]

For technical desulfurization (especially for vacuum desulfurization treatment), the slag composition is adjusted to reach the lime saturated slag before vacuum treatment. If the slag is undersaturated, lime is added. In the case of superaturated slag, alumina or silica is added. The quantity of addition depends on the saturation index. This adjustment of a lime-saturated slag might lead to a desulfurization potential of more than 10000 that can be seen in Figure 2.2 and this is equivalent to a sulfur partition ratio about 1000 [17].

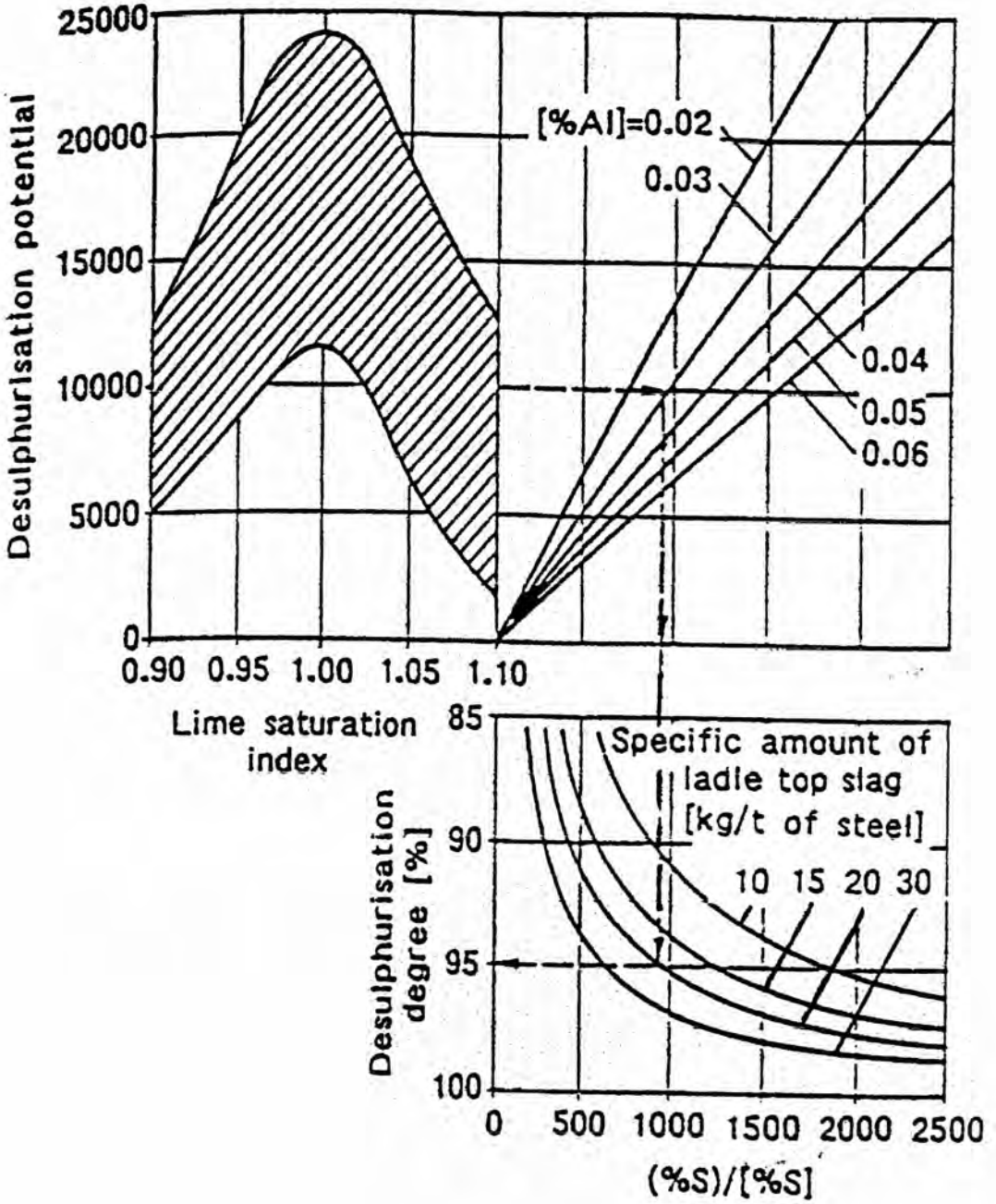

Figure 2.2 Desulfurization depends on lime saturation index, aluminium content and the specific slag amount [17]

The desulfurization reaction for lime-aluminate slag can be written as [17,19,20] :

$$[S] + 2/3[Al] + (CaO) = (CaS) + 1/3(Al_2O_3) \quad (2.1)$$

or

$$[S] + (CaO) = (CaS) + [O] \quad (2.2)$$

and when the steel contains strong deoxidized elements (e.g. Al) consequently,

$$2[Al] + 3[O] = (Al_2O_3) \quad (2.3)$$

Consequently, the overall reaction of (2.2) and (2.3) is as same as Eq.(2.1).

Eq.(2.1) enables the definition of the desulfurization potential which is shown in Figure 2.2. According to Figure 2.2, lime saturated slag has the highest desulfurization potential. Undersaturated and supersaturated slags lead to reduction in the desulfurization potential.

Desulfurization degree (η_s) is defined by Eq.(2.4).

$$\eta_s = \frac{[S_i] - [S_f]}{[S_i]} \times 100 \quad (2.4)$$

where $[S_i]$ is the initial sulfur content and $[S_f]$ is the final sulfur content in the steel.

η_s is influenced by ladle top slag composition, slag amount, aluminium content in the treated steel, treatment time for desulfurization and stirring condition [17, 18, 21].

The desulfurization degree can be directly transferred from desulfurization potential as also shown in Figure 2.2, e.g. the desulfurization potential with 0.03%Al-content and a specific slag amount of 20 kg/t.steel under this circumstance a sulfur mass balance reaches 95% degree of desulfurization. Consequently, for operationally reliable achievement of the maximum degree of desulfurization it is necessary to have an exactly adjusted lime saturated ladle top slag [17].

The equilibrium for Eq.(2.1) is expressed by Eq.(2.5), desulfurization potential:

$$\frac{(\%S)}{[\%S]\cdot[\%Al]^{2/3}} = \frac{K_1^{*}\cdot a_{CaO}}{a_{Al2O3}^{1/3}} \qquad (2.5)$$

where (%S), [%S] is the percent sulfur in the slag and steel, respectively,

[%Al] is percent aluminium in steel, a_{CaO} and a_{Al2O3} is the activity of CaO and Al_2O_3 in the slag, respectively, K_1^* is the equilibrium constant of Eq.(2.1).

Eq.(2.5) relates to sulfide capacity (reference to the 1wt.% solution in the metal phase), C'_s. The highest sulfide capacity is the highest sulfur distribution between slag and steel, (%S)/[%S], and equivalent to the highest desulfurization degree.

The sulfide capacity can be expressed by reference to the 1wt.% solution in the metal phase [15,22-29].

$$C'_s = (a_{[o]}/a_{[s]}) / (wt\%\ S) \qquad (2.6)$$

where $a_{[o]}$ and $a_{[s]}$ are respectively the activities of oxygen and sulfur in the metal phase.

IRSID [30] presented the slag model which has been used to calculate the sulfur partition coefficient between slag and metal, Ls, according to the following equation :

$$L_s = (\%S)_{slag} / [\%S]_{metal} = C'_s/(f_{[s]}.a_{[o]}) \qquad (2.7)$$

where $f_{[s]}$ is a Henrian activity coefficient of sulfur in the metal phase.

Iso-sulfur partition diagram from the calculation according to the IRSID slag model for the system $CaO-Al_2O_3-SiO_2$ and the oxygen activity is fixed by the equilibrium $[\%Al]/(\%Al_2O_3)$ with $a_{[Al]} = 0.03$ and temperature is 1600 °C as shown in Figure 2.3.

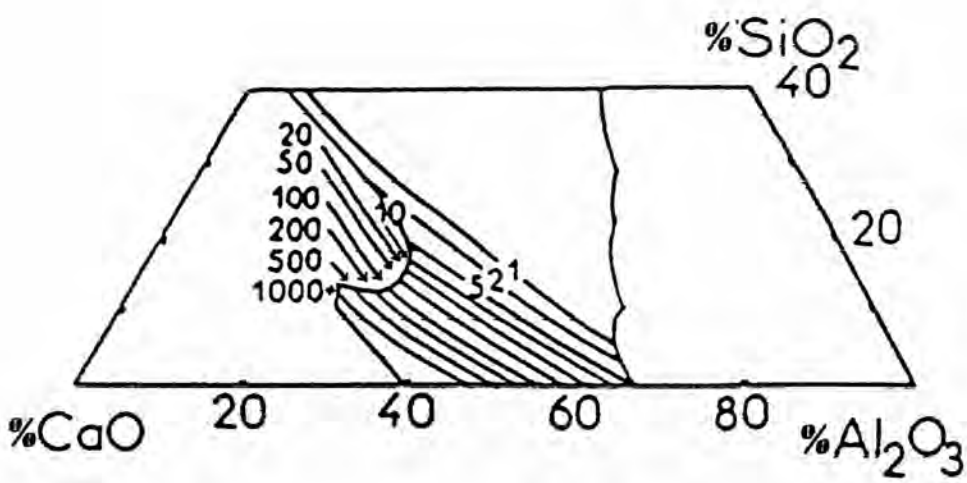

Figure 2.3 Calculated sulfur partition coefficient between slag and metal at 1600 °C [30]

The sulfide capacities of $CaO-Al_2O_3-SiO_2$ slag increase with increasing temperature, concentration of CaO and Al contents in the metal.

Many factors affect on desulfurization reaction. Generally, the following optimized conditions should be fulfilled:

1) Basic slag with high sulfide capacity, high CaO activity in the ladle slag which can be obtained by lime saturated slag

2) Low oxygen content in the molten steel which can be obtained with the following:

   2.1) Steel desulfurization is carried out under the reducing condition

   2.2) Treated steel contains strong deoxidized elements (e.g. Al). This is one reason why killed steel can remove sulfur better than unkilled steel.

3) Strong stirring condition that can provide under vacuum condition. In Tank Degasser (TD), VOD and other vacuum facilities, the steel can be intensively stirred without oxidation results in increasing slag/molten steel interface and accelerate the mass transport of sulfur. These results enhance the desulfurization kinetic.

4) High treatment temperature because the desulfurization is an endothermic reaction.

5) High slag amount which leads to more sites in the slag to contain sulfur.

2.2.2 Denitrogenization

Recently a more stringent control of the nitrogen level in steel has become of great interest for new types of products such as cold rolled sheets produced by the continuous annealing process where lower carbon and nitrogen levels are required. Corresponding to this trend, fundamental studies of the mechanism of nitrogen desorption and absorption have been made by several investigators. At first, nitrogen adsorption and desorption were treated simply as a first or second order reaction with respect to the nitrogen content in the melt. It was found that, in the case of low oxygen and sulfur content, nitrogen desorption obeys the second order and nitrogen absorption a first order reaction model. It is well known that the second order reaction coefficient is dependent on the content of surface active elements [31-33].

Currently, beside nitrogen removal during degassing process, there is no efficient way to remove nitrogen. Vacuum degassing including argon gas stirring has been developed to decrease the amount of nitrogen in the treated steel to the desired values [8].

The equation of nitrogen desorption can be written as:

$$[N] + [N] = \{N_2\} \quad (2.8)$$

The simple rate of reaction in the case of low nitrogen (less than 100ppm N) and high oxygen level is expressed by the following equation [31]:

$$-dN/dt = \left([N]^2 - [N]_e^2\right) \cdot k_1 \cdot A/V \quad (2.9)$$

where [N] is the nitrogen content in the steel, the subscript 'e' denotes the equilibrium, $\{N_2\}$ is the nitrogen in gas phase, k_1 is the rate constant of the interfacial reaction, A/V is the ratio of gas/liquid interface to the volume of molten steel.

Harashima *et. al.* [34] presented the nitrogen removal rate from liquid iron which can be approximated by a second order reaction according to Eq. (2.9), but the interfacial rate constant (k) would be the overall rate constant, nitrogen mass transfer and interfacial reaction.

Harada and Janke [35] described denitrogenization under the reduced pressure in the term of mixed control model, liquid-gas phase mass transfer and

chemical reaction at the interface, Figure 2.4 [17,35]. The reaction rates of the three steps are expressed as follows:

liquid phase mass transfer:

$$\frac{dn_{N_2}}{dt} = k_L A \frac{\rho_L}{100 M_{N_2}}([\%N] - [\%N]_i) \tag{2.10}$$

chemical reaction at the interface:

$$\frac{dn_{N_2}}{dt} = k_c A \frac{\rho_L}{100 M_{N_2}}([\%N]_i^2 - [\%N]_e^2) \tag{2.11}$$

gas phase mass transfer:

$$\frac{dn_{N_2}}{dt} = k_G A \frac{p}{RT} \ln \frac{p - p_{N_2}}{p - p_{N_{2,i}}} \tag{2.12}$$

From these equations, the following differential equations can be derived:

$$\frac{d[\%N]}{dt} = -k_L A / V([\%N] + \alpha/2 - \sqrt{\alpha[\%N] + (\alpha/2)^2 + K^2 p_{N_2}} \tag{2.13}$$

where $\alpha = k_L(\frac{1}{k_C} + \frac{1}{k_G}\frac{\rho RTK^2}{100 M_{N_2}})$

A reaction surface area (cm^2)

K equilibrium constant, $K = [\%N] / P_{N_2}^{0.5} = \frac{0.0447\%}{bar^{0.518}}$

k reaction rate

P total pressure

R gas constant (82.057 cm^3 bar/mole K)

T temperature

t time (s)

n_{N_2} transferred nitrogen moles (mol)

M_{N_2} mole weight of nitrogen (g/mol)

[%N] nitrogen content in metal (wt.%)

$[\%N]_i$ nitrogen content in metal at the interface (wt.%)

$[\%N]_e$ nitrogen content in the metal in equilibrium with the nitrogen partial pressure at the interface (wt.%)

ρ_L density of molten iron at 1600 °C (7.0 g/cm^3)

subscripts i denotes at interface

e denotes at equilibrium

The mixed control model is applicable for both nitrogen desorption and absorption. The α value consists of three coefficients and can be written as follows at 1600 °C:

$$\alpha = k_L(\frac{1}{k_C} + \frac{0.77}{k_G}) = \frac{k_1}{k_2} \qquad (2.14)$$

where $k_1 = k_L$, $k_2 = (1/k_C + 0.77/k_G)^{-1}$

k_1 is the first order and k_2 the second order reaction coefficient.

Bannenberg *et al.* [17] investigated denitrogenization in the tank degassing unit, denitrogenization takes place predominantly during argon bubble rising in the liquid steel (see Figure 2.5). Gas extraction from the melt can be described as follows. At the bottom of the ladle the nitrogen partial pressure in the argon bubble is zero. Nitrogen from the bulk liquid steel will be adsorbed into the bubble, according to the Sieverts' law ($[N] = KP_{N2}^{1/2}$), until the nitrogen partial pressure in the argon bubble is in equilibrium to the bulk steel. At the bottom of the ladle the total pressure is very high due to the ferrostatic pressure, only small amount of nitrogen can be drained into the bubble. The ferrostatic pressure decreases constantly during argon bubble rises higher so that the nitrogen in the melt is adsorbed into the bubble.

The transfer of nitrogen between the liquid steel and the injected argon bubble can be represented by a mixed control model, taking into account the two elementary steps: liquid phase transfer and interfacial reaction as shown in Figure 2.4.

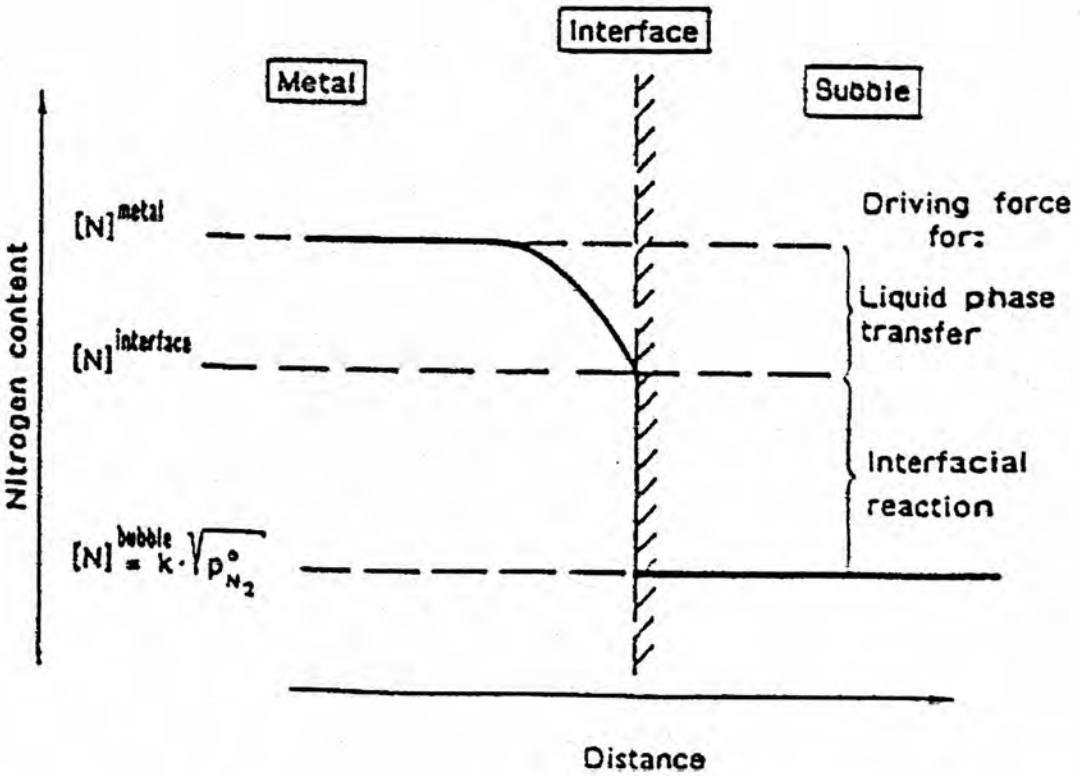

Figure 2.4 Concentration profile of nitrogen at the bubble/metal interface [17,35]

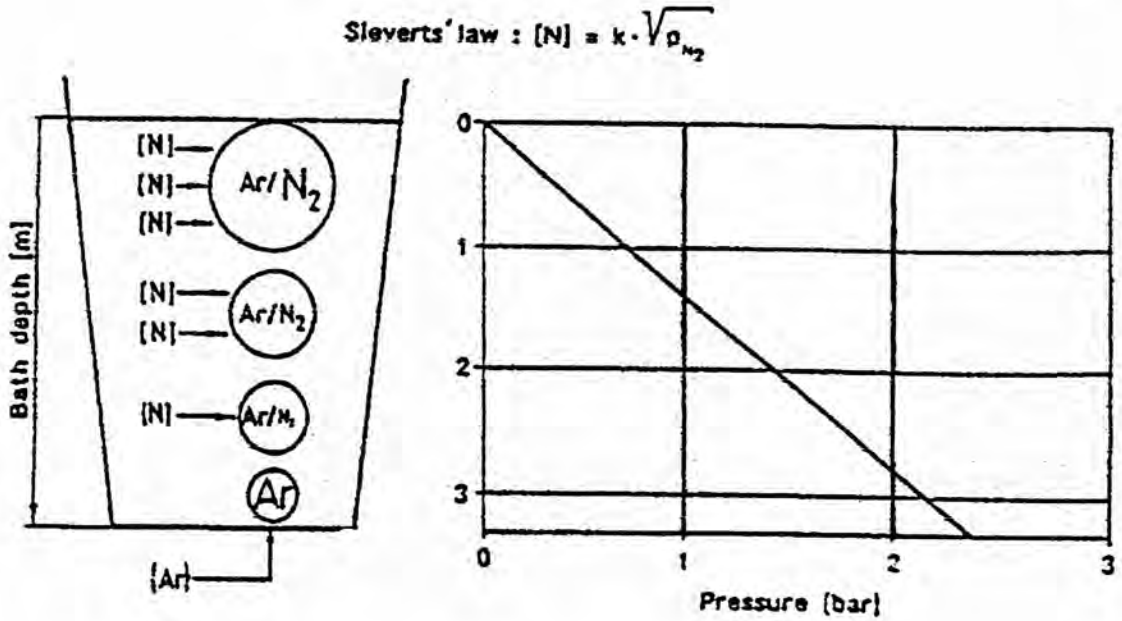

Figure 2.5 Schematic representation of denitrogenization by argon and local pressure during vacuum treatment [17]

Figure 2.6 illustrates the strong decrease of nitrogen with increasing argon stirring gas volume for 185 tons steel. Higher nitrogen content before the vacuum treatment leads to higher nitrogen content at the end of the treatment for a constant argon stirring volume. The higher amount of argon volume leads to the lower nitrogen content in the vacuum treatment for a constant initial nitrogen content before vacuum treatment. Therefore the lowest nitrogen content after vacuum treatment is obtained by a low nitrogen content before vacuum treatment and high amount of argon stirring gas volume.

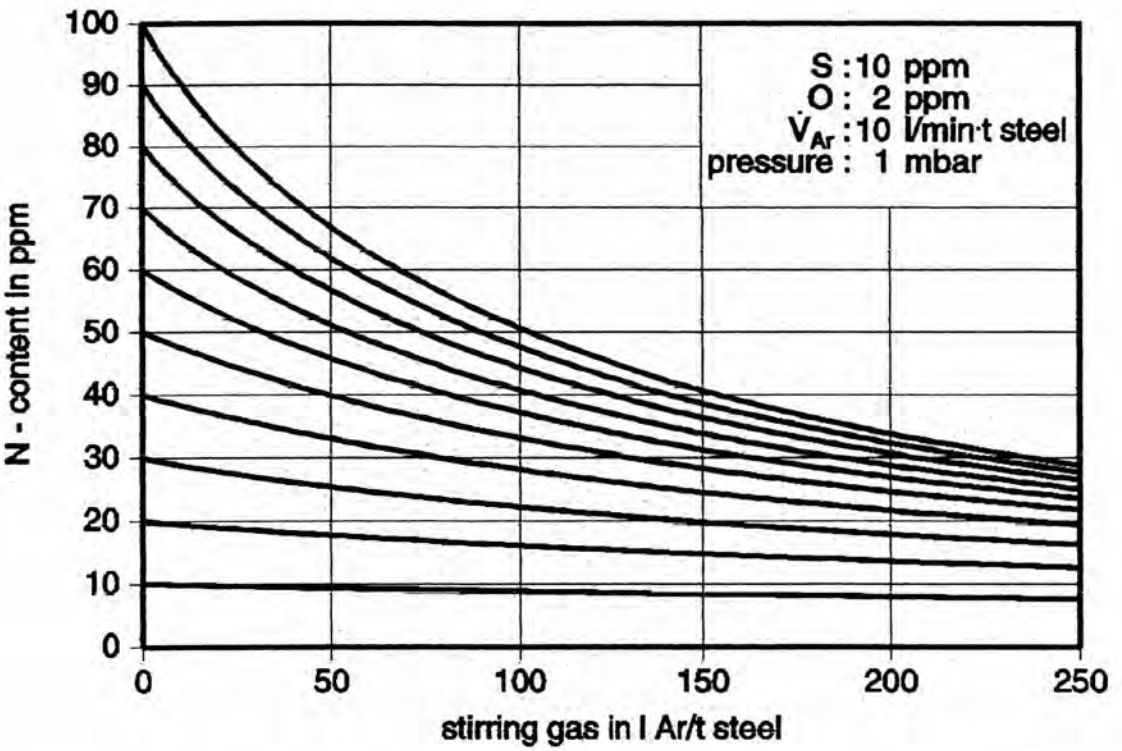

Figure 2.6 Decrease of nitrogen content during vacuum treatment [17]

Kitamura *et. al.* [36] presented the model for nitrogen desorption and decarburization reaction in VOD process. The reaction sites of the nitrogen desorption reaction are considered as:

1) bath surface except the hot spot by oxygen blowing because of high oxygen potential
2) the surface of the injected argon bubble and
3) the surface of CO gas bubble formed inside the bath, as shown in Figure 2.7.

The rate of nitrogen desorption reaction is controlled by both the mass transfers of nitrogen in the molten steel and the chemical reaction at the surface. The mass transfer rate of nitrogen molecules in the gas phase is neglected because its rate is much larger than the rates under low pressure. The nitrogen desorption mainly occurs at the surface of CO gas bubble when CO gas formation in the bath takes place strongly in the early stage of oxygen blowing operation. When CO gas formation decreases, about 70% of the nitrogen desorption occurs at the bath surface and about 30% of the reaction takes place at the surface of the injected argon bubble.

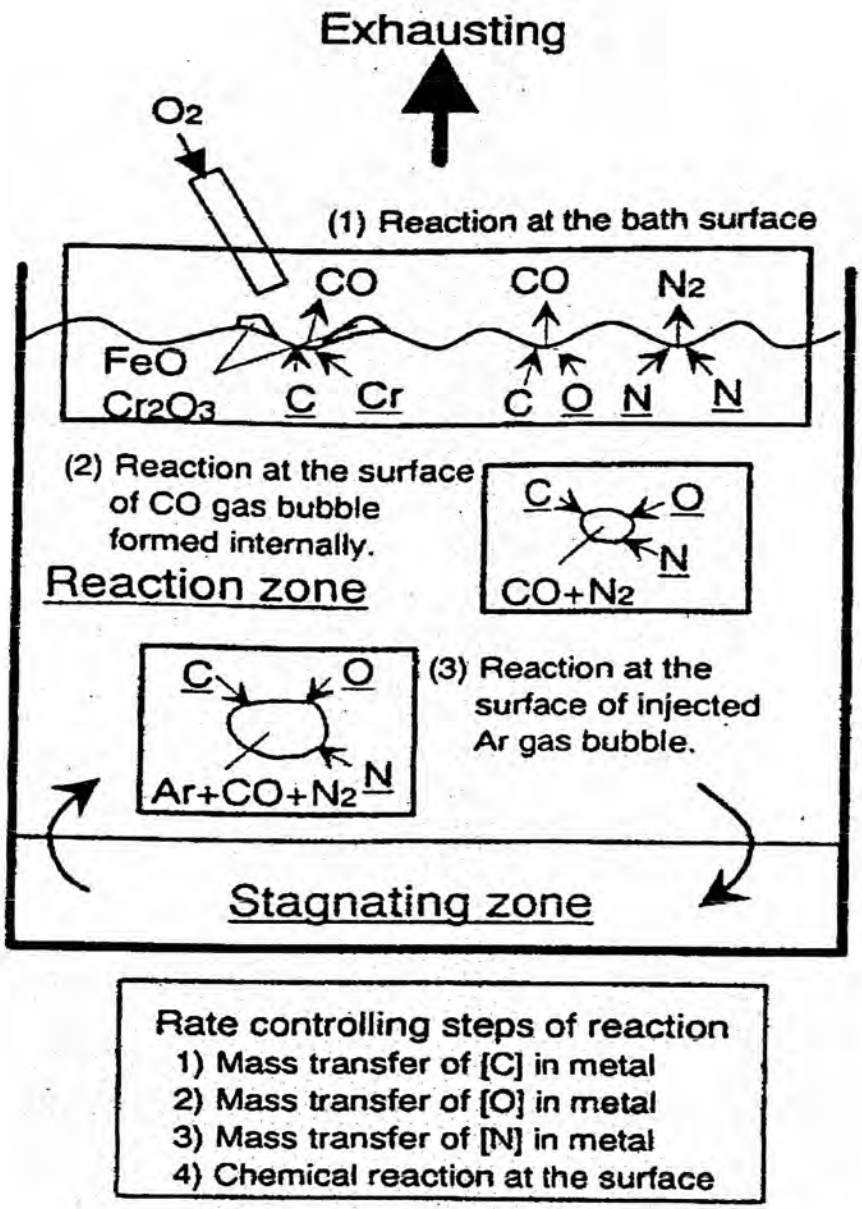

Figure 2.7 Outline of decarburization and nitrogen desorption model [36]

Geller's equation can be used to estimate the quantity (Q_i in mole) of purge gas required per gram atom of nitrogen [37]:

$$Q_i = \frac{1}{2} \cdot \left[\frac{1}{P_{N2}^{\bullet} \cdot N^{\bullet}} - 1 \right] \cdot \left[1 - N^{\bullet} \right] \qquad (2.15)$$

where $P_{N2}^{\bullet} = \left(\frac{\%N^o}{K_{N2}} \right) \cdot \frac{1}{P_{tot}}$, $N^{\bullet} = \frac{\%N}{\%N^o}$ and superscript 'o' denotes a concentration before the purging.

The quantity Q_i may be converted to more practical volume units, V_i as follows:

$$V_i = 575 Q_i (\%N^o) \qquad \text{ft}^3\text{/t.steel} \qquad (2.16)$$

The rate of nitrogen desorption is strongly influenced by the surface active elements, such as sulfur and oxygen. The depression of the rate is caused from the blockage at the interfacial site by such surface active elements.

Many factors must be considered for denitrogenization. In general, the denitrogenization could be successfully obtained in vacuum degassing unit with the following:

1) Low initial nitrogen content before vacuum treatment
2) Low surface active elements in the treated steel in particular for sulfur and oxygen
3) Low atmospheric pressure in vacuum degassing unit
4) High amount of stirring argon and low stirring rate
5) High purity of argon stirring (avoidance of the use of nitrogen entrained argon gas)

The new tendency for nitrogen refining by slag or flux mixtures with high nitride capacities have been investigated by several workers [8,22,38,39]. The fundamental of slag denitrogenization and prevention of nitrogen pickup as well as the elaboration of technological parameters for effective nitrogen removal from steel are emphasized to the nitrogen solubility in various slag mixtures and the measurement of the nitride capacities as well as the calculation of nitrogen distribution ratios between slag and liquid metal.

Utochkin *et. al.* [38] studied the possibility of nitrogen refining by slag or flux mixtures with high nitride capacities by ladle treatment of steel. They presented the nitrogen solubility and nitride capacities in Al_2O_3-CaO-TiO_2 and

CaF_2-TiO_2 systems. The presence of 10 wt-% TiO_2 in Al_2O_3-CaO slag markedly enhances the nitrogen solubility of the slag. With the addition of TiO_2, the nitride capacity (C_N) of 50CaO-50Al_2O_3 slag increases from 5.38×10^{-14} to 4.31×10^{-13} at 1873 K. The highest C_N has been found in 60CaO-40TiO_2 flux, equal to 2.34×10^{-12} at 1873 K.

Yamanaka *et. al.* [39] investigated nitrogen desorption from molten steel by flux treatment regarding the flux of the CaO-Al_2O_3-CaF_2-BaF_2-SiO_2-MgO system. They found that nitrogen transfer from the molten steel to gas was promoted with decreasing surface active elements, such as oxygen and sulfur, by using the mentioned flux. The nitrogen desorption is controlled by the interfacial chemical reaction rate when O+S/2 is lower than 0.004. Above 0.004, the nitrogen desorption is controlled by the mass transfer in the metal phase.

2.2.3 Decarburization

The decarburization during secondary metallurgical treatment is obviously achieved. The involved reactions of decarburization can be concluded as:

$$[C] + [O] = \{CO\} \quad (2.17)$$

$$2[C] + \{O_2\} = 2\{CO\} \quad (2.18)$$

$$\{CO\} + 1/2\{O_2\} = \{CO_2\} \quad (2.19)$$

$$[C] + \{O_2\} = \{CO_2\} \quad (2.20)$$

$$[C] + (FeO) = \{CO\} + Fe \quad (2.21)$$

The C-O equilibrium of Eq.(2.17) at 1600 °C can be expressed by Eq.(2.22) [1].

$$[\%C]\cdot[\%O] = 0.0025P_{CO} \quad (2.22)$$

In general, decarburization reactions are favored by oxidizing condition. From Eq.(2.17) the promoting conditions are higher oxygen content in the steel and lower CO partial pressure in the vacuum vessel. Lower CO partial pressure can be provided under vacuum treatment. Higher oxygen

potential can be obtained by: unkilled tapping steel from EAF to keep dissolved oxygen in the treated steel, the other way is oxygen blowing that can be performed in VOD.

In general, the treated steel is adjusted for the oxygen potential to the path of decarburization instead of deoxidation path which can be seen from the C-O equilibrium.

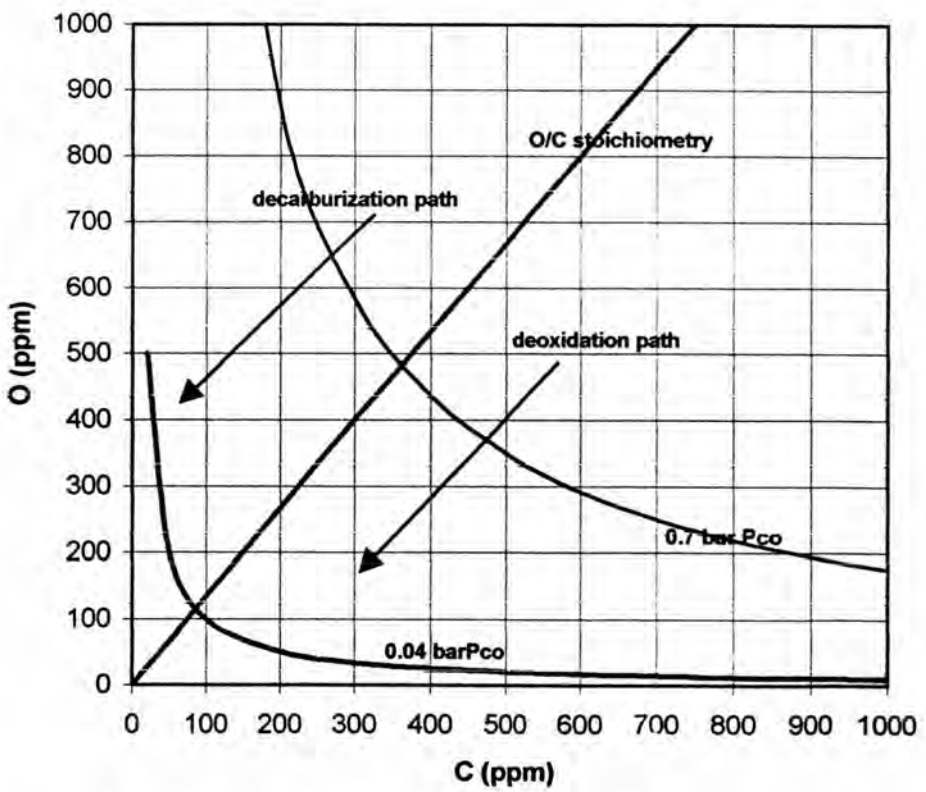

Figure 2.8 C-O equilibrium diagram at 1600 °C

Many factors involve decarburization reactions. The rate of reactions are governed by [40] :

1) Rate of diffusion of carbon from the bulk steel to reaction sites,
2) Rate of diffusion of oxygen from the bulk steel to reaction sites,
3) Rate of C-O reaction (CO formation) at the reaction sites,
4) Rate of CO removal (CO evolution) from the steel bath

The rate of decarburization is determined by the slowest or a combination of slower steps. It is complicate to point out which rate is controlling the reaction. Many workers have studied the decarburization for several conditions and several decarburization facilities. They found that the rate of decarburization under reduced pressure is determined by the following factors:

1) diffusion coefficient
2) motive force for the reaction, this is defined by concentration gradient between the equilibrium concentration on the reaction site and the momentary concentration of carbon in the bulk of the molten steel
3) effective degassing surface for CO evolution
4) the flow condition of molten steel, this is defined by the thickness of the boundary layer on the site of the molten steel at the gas/metal interface.

The decarburization reaction might be controlled by the rate of carbon diffusion through the above-mentioned boundary layer. Carbon and oxygen content and temperature of the molten steel, pressure in the vacuum system and the flow rate of argon gas are the predominant factors [41].

RaO and Lee [42,43] studied the effect of surface active elements on decarburization mechanism in the Fe-C alloys. The surface active elements (S, O) have virtually no effect on the decarburization. Also the work of Kishimoto *et al* [44], indicated that no significant effect of sulfur content on the decarburization rate with carbon content of more than 10 ppm. With carbon content of less than 10 ppm, the decarburization rate decreases with increased sulfur content. The effect of sulfur content on the decarburization rate is, however, very small even with carbon content of less than 10 ppm. It was reported that the effect of sulfur on the decarburization rate was not observed with carbon content more than 10 ppm since the chemical reaction at gas-metal interface was not the rate determining step.

Najafabadi *et. al.* [45] defined the rate of decarburization under vacuum as the first order rate according to the following:

$$\ln\frac{\left([ppmC]-[ppmC]_f\right)}{\left([ppmC]_o-[ppmC]_f\right)}=k_c^{'}\cdot A/V\cdot t \qquad (2.23)$$

where [ppmC] is the carbon content of the melt, $k_c^{'}$ is the overall apparent first order rate constant, A/V is a ratio of total area of the reaction interface to the volume of the melt, t is time and subscript "o" and "f" denote the initial and final values.

Deo *et. al.* [46] and Yamaguchi *et. al.* [47] developed models based on mass transport of carbon or mixed mass transport of carbon and oxygen in the RH degassing unit (vacuum circulation process). Mass transport of carbon and oxygen in the metal phase can be considered to be the two rate controlling steps during decarburization in the RH vessel. According to the laboratory experiments conducted by Suzuki, the decarburization rate is only controlled by mass transport of carbon when the mass ratio of [C]/[O] is less than 0.52. At the mass ratio greater than 0.52 the decarburization rate is controlled by mass transport of oxygen. In the actual processes the mass ratio at the start of the treatment in RH vessel is approximately 0.5 and it is reduced towards the end of the treatment to less than 0.3. Obviously, for the conditions when the ratio is close to 0.52, the model can be based on the assumption of the mass transport of carbon and oxygen (i.e. mixed mass transport control). As the carbon contents

drop with the treatment time, carbon mass transport control will become more and more predominant.

Takayashi *et. al.*[48] developed a mathematical model for decarburization in RH degasser. The decarburization through argon and CO bubbles in the molten steel, and the free surface can be estimated separately. The contribution of decarburization through three interfaces to the total decarburization is shown in Figure 2.9. Decarburization through argon bubbles contributes a lot in the first stage and the contribution of decarburization as CO bubbles is very large throughout the operation. They found that a small decarburization rate at the end of the operation results from little formation of CO bubbles.

Ermoleava *et. al.*[49] investigated the characteristics of decarburization of metal during continuous vacuum degassing. Evidently during vacuum degassing of metal with a very low carbon concentration, the decarburization process is limited by the supply of carbon to the reaction site. The delivery of argon is the issue of the increase of reaction surface, thus the continuous argon vacuum treatment will be possible to make the intensive decarburization.

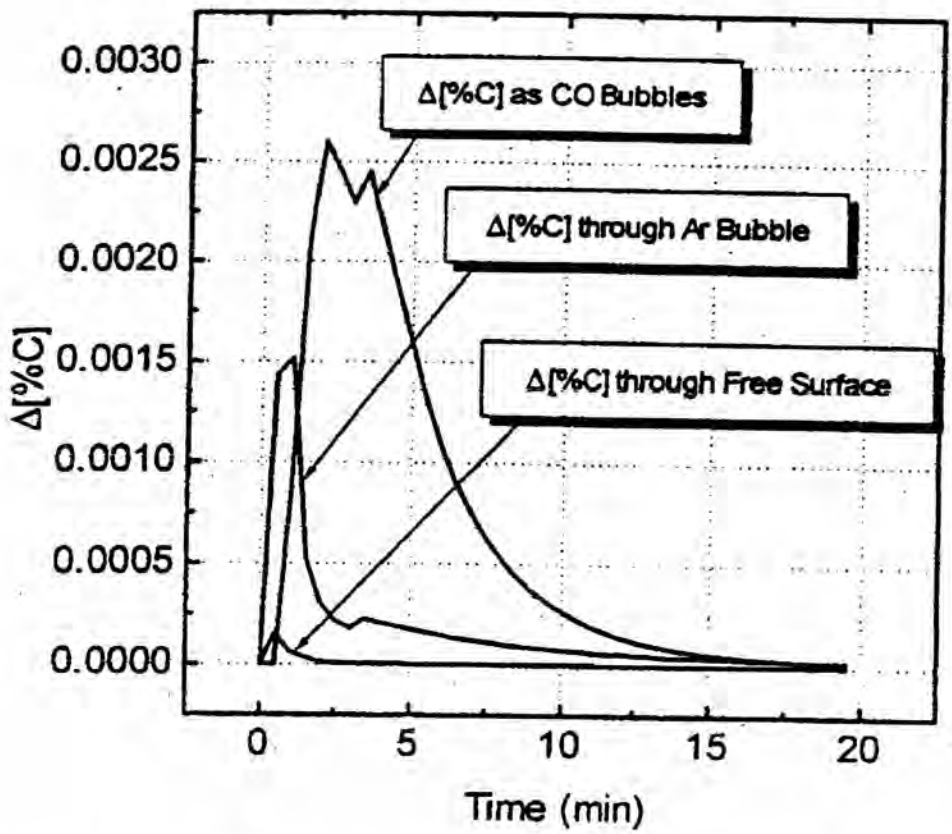

Figure 2.9 Decarburization at each reaction site during vacuum treatment of the RH process [48]

Bannenberg *et. al.*[50] investigated the decarburization in the vacuum tank degasser. Decarburization is assumed to be a first order reaction which can be expressed by the equation:

$$\ln\frac{C}{C_o} = -k \cdot t \qquad (2.24)$$

where C and C_o is the final carbon content and initial carbon content, respectively.

k is the apparent kinetic constant in min^{-1}.

t is the treatment time in minute.

The carbon evolution seems to be composed of three periods:

1) The first period where no remarkable decarburization occurs. The duration of this period varies from one to three minutes.

2) The following second period, a strong natural decarburization takes place down to carbon contents in the range of 70 ppm. During this period the bath agitation is maximum.

3) Finally an inert gas driven decarburization takes place below 4 mbar. The efficiency of this mechanism seems to be related to the stirring argon flow rate.

Figure 2.10 shows the typical evolution gas analysis during vacuum treatment after starting the evacuation.

Figure 2.11 shows the feature of decarburization during the vacuum decarburization treatment. The rate of carbon removal after starting the evacuation through the end of vacuum treatment can be assumed to be the first

order reaction, consists of two kinetic constants which gives a good description of the decarburization occurring in industrial vacuum processes.

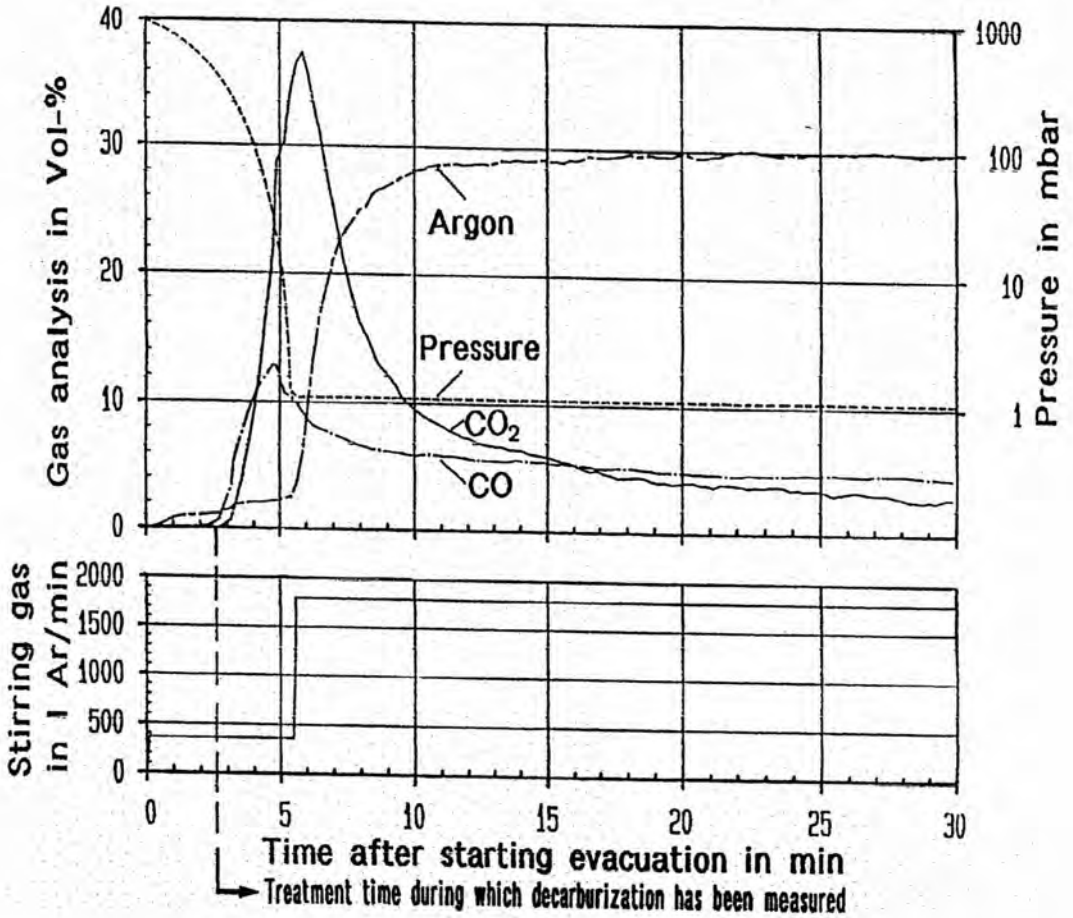

Figure 2.10 Evolution gas analysis during vacuum treatment in TD [50]

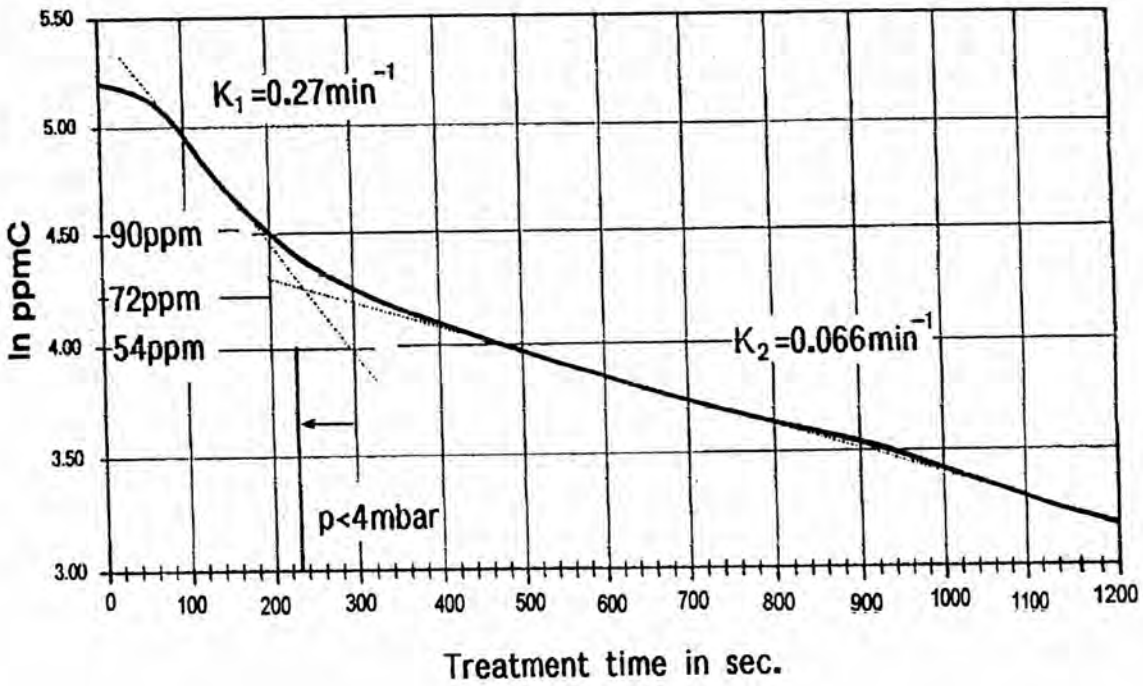

Figure 2.11 Calculated remaining carbon content as a function of time (logarithmic scale) during vacuum treatment in TD [50]

The carbon and oxygen drop are nearly stoichiometric to the CO formation. The final carbon and oxygen contents correspond to the CO partial pressure of about 40 mbar, which is about 20 times bigger than the final pressure in the tank degasser. The nearly stoichiometric CO formation can be seen in Figure 2.12 in which a comparison between the initial measured oxygen content and the equivalent oxygen content (Eq. (2.25)).

$$O_{equivalent} = O_{final} + \frac{16}{12}\Delta C \qquad (2.25)$$

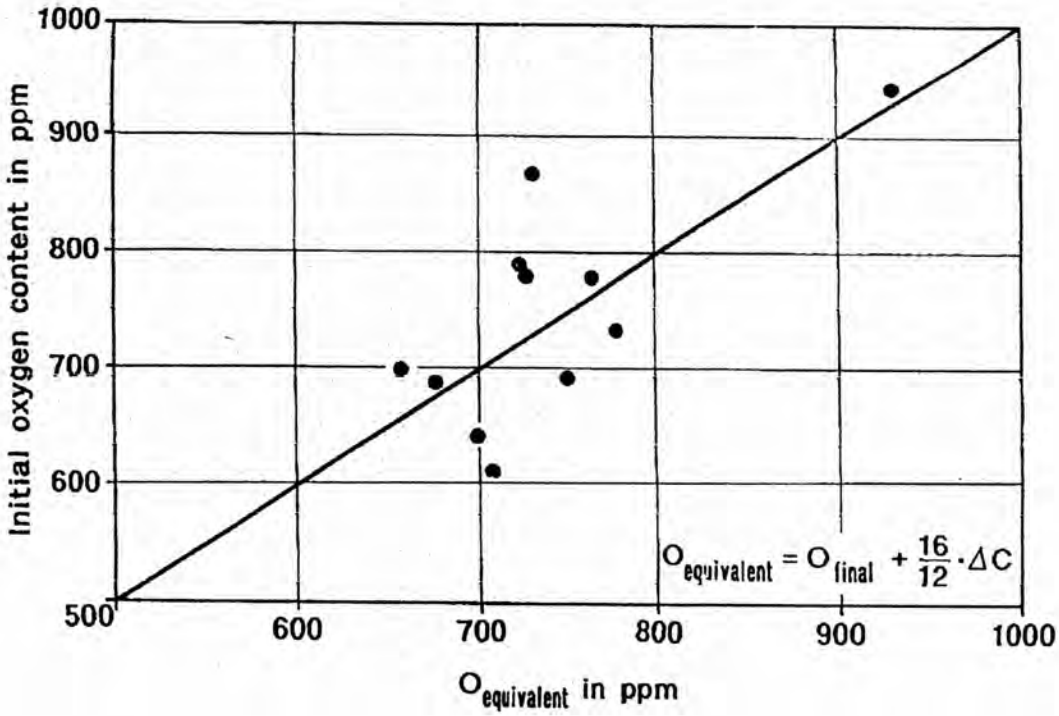

Figure 2.12 Comparison between calculated and measured initial oxygen content [50]

Reichel *et. al.*[51] and Reichel [52] presented the measurement of the decarburization rate by using waste gas measurements and using the fact that the waste gas consists mainly of gaseous products from the reaction in the metal bath, i.e., CO and CO_2. The rate of decarburization can be calculated from K_{CO} and K_{CO2} concentrations and the flow rate of waste gas Q_G , as follows:

$$-\frac{dc}{dt} = k \cdot \left(Kco + Kco_2\right) \cdot Q_G \qquad (2.26)$$

where k is the rate constant of decarburization, Kco and Kco_2 is a concentration of CO and CO_2 in waste gas, respectively, Q_G is flow of waste gas

The decarburization reaction takes place giving CO formation which constituted approximately 80% of the waste gas (see Figure 2.13). Approximate 20-25% of the ascending CO bubbles underwent post combustion. The resulting waste gas consists of 60% CO and 20% CO_2. A slight loss of the ceramic consumable oxygen lance head leads to a slight decrease in CO content and a simultaneous increase in the CO_2 content.

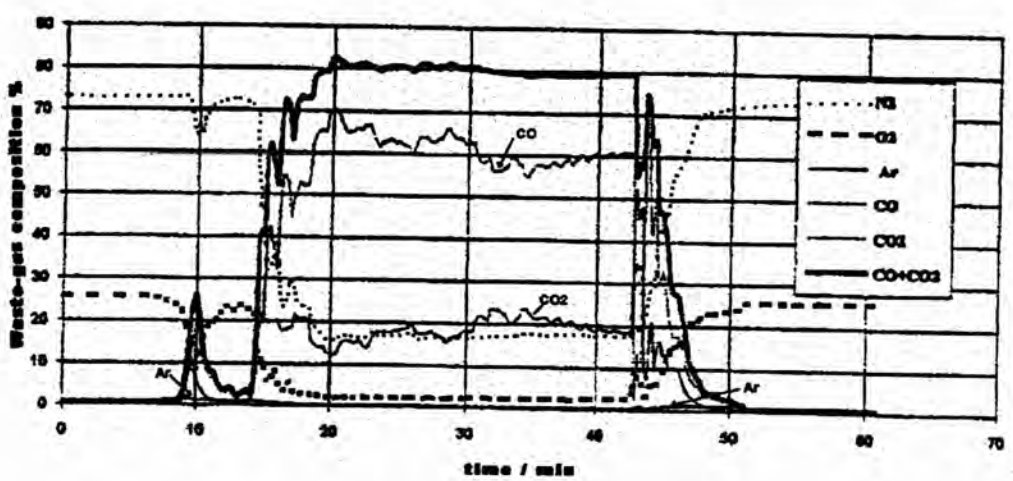

Figure 2.13 Waste gas composition from VOD [51]

Referring to Figure 2.14, about 20% of the CO which is obtained in the metal bath is converted to CO_2. The post combustion is more effective with greater dispersive character of the blowing stream and with larger reaction scope for post combustion. The optimization of oxygen blowing is connected to the optimized bath depth and oxygen lance position.

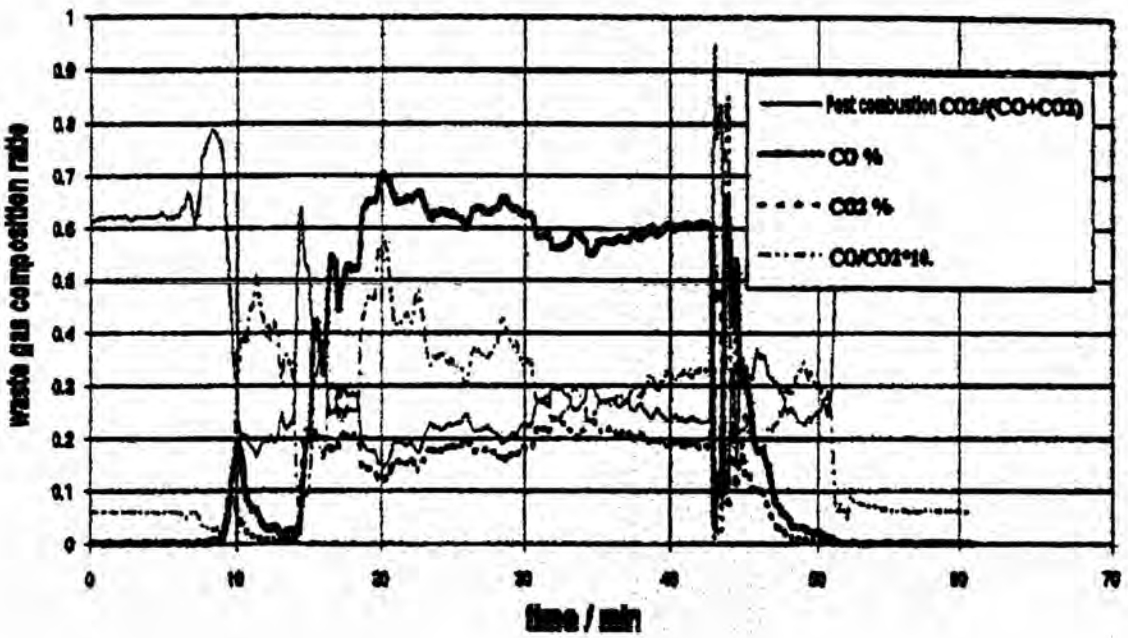

Figure 2.14 Post combustion ratios in the facility [51]

In the VOD process the lowest final carbon content accompanied by the efficient using of oxygen blowing is one of the main criteria for the effectiveness of the process. The vacuum treatment combined with oxygen blowing can reach optimum conditions for decarburization. With adequate oxygen blowing to adjust oxygen potential, low CO partial pressure and

sufficient time, the carbon content less than 30 ppm can be achieved in this vacuum facility.

2.2.4 Temperature control during secondary metallurgical treatment

The level and uniformity of steel superheating during casting are decisively important for the quality of the casted steel. Exact adjustment of the required steel temperature over the complete process of the steel works and right up to the casting is ensured by mean of a temperature control [53].

The cooling behavior of the steel from the melting unit (e.g. EAF) to casting is mainly driven by:

- temperature losses during tapping and
- temperature losses during secondary treatment

The temperature losses during tapping are mainly composed of radiation losses from the tapping stream and the free surface of the heat as well as the heat required for heating and melting the alloying agents. Heat is then extracted from the steel in the ladle through:

- radiation losses over the bath surface
- thermal conduction through the refractory lining in the wall and bottom of the ladle and

- heating of the refractory lining of the ladle.

The industrial practice in Dillinger Huette GTS/Germany, a ladle cover is used during the complete secondary metallurgical process and during casting as well as during the empty ladle period. The cover is only removed during the steel tapping from the melting unit. The cover is used to reduce the temperature loss of the steel melt by radiation through the bath surface and particularly the cooling of the refractory during the empty ladle time. The surface temperature decrease is substantially stronger when there is no cover on the empty ladle than the covered ladle. This decrease in temperature of the initial ladle wall naturally leads to a decrease in a total heat content of the refractory lining and consequently a higher cooling down of the steel. With empty ladle periods in excess of 180 minutes the covered ladle is subjected to heat which enables the surface to be maintained at a relative high temperature. On account of the reproducible conditions regarding the heat content of the ladle by using the ladle cover, cooling of the steel in the ladle is substantially only dependent on the empty time of the ladle. The functional relationship between the two parameters is given by [53]:

$$\Delta T = (a + b\sqrt{LZ}) \cdot t^{0.65} \qquad (2.27)$$

where ΔT = decrease in temperature of the steel melt in °C/min

a, b = operating constants

LZ = empty ladle time in minute

t = time in minute

Figure 2.15 shows the occurring cooling conditions of the steel in relation to its resident time in the ladle for different empty ladle times. For the empty ladle time longer than 180 minutes the ladle is heated, therefore temperature loss over the longer periods are not greater than that occur of 180 minutes.

When there is no possibility to heat the steel in the ladle, e.g. in a ladle heating furnace, the tapping temperature has to be reliably adjusted. However, it is necessary to avoid a tapping temperature that is distinctly above the target temperature. Too high tapping temperature primarily leads to an increase in refractory wear in the melting unit and the ladle.

Figure 2.16 shows an example of the temperature development of the melt from the end of the blowing process to the tundish. The time from the end of converter tapping up to start of casting takes only 65 minutes. The converter tapping temperature is 1670 °C. Due to the addition of alloying and slag forming agents, the temperature in the ladle directly drop after tapping down to 1620 °C. At the start of the casting the temperature is 1568 °C.

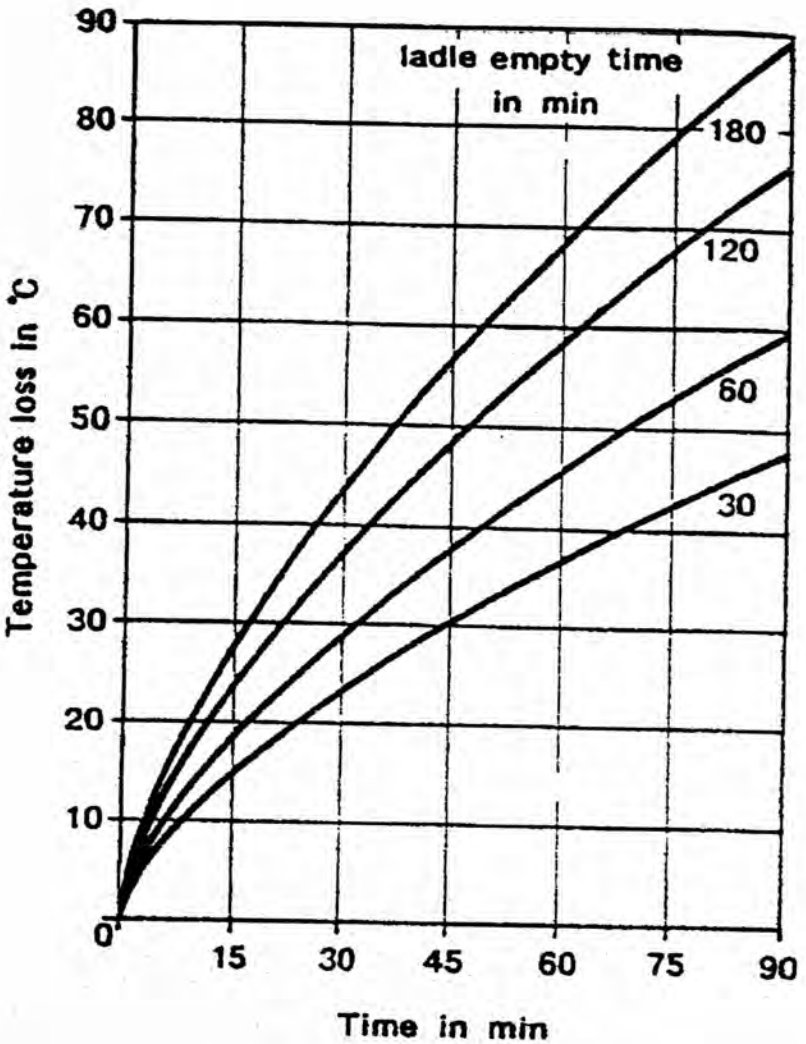

Figure 2.15 Steel temperature loss dependent on time for different ladle empty times [53]

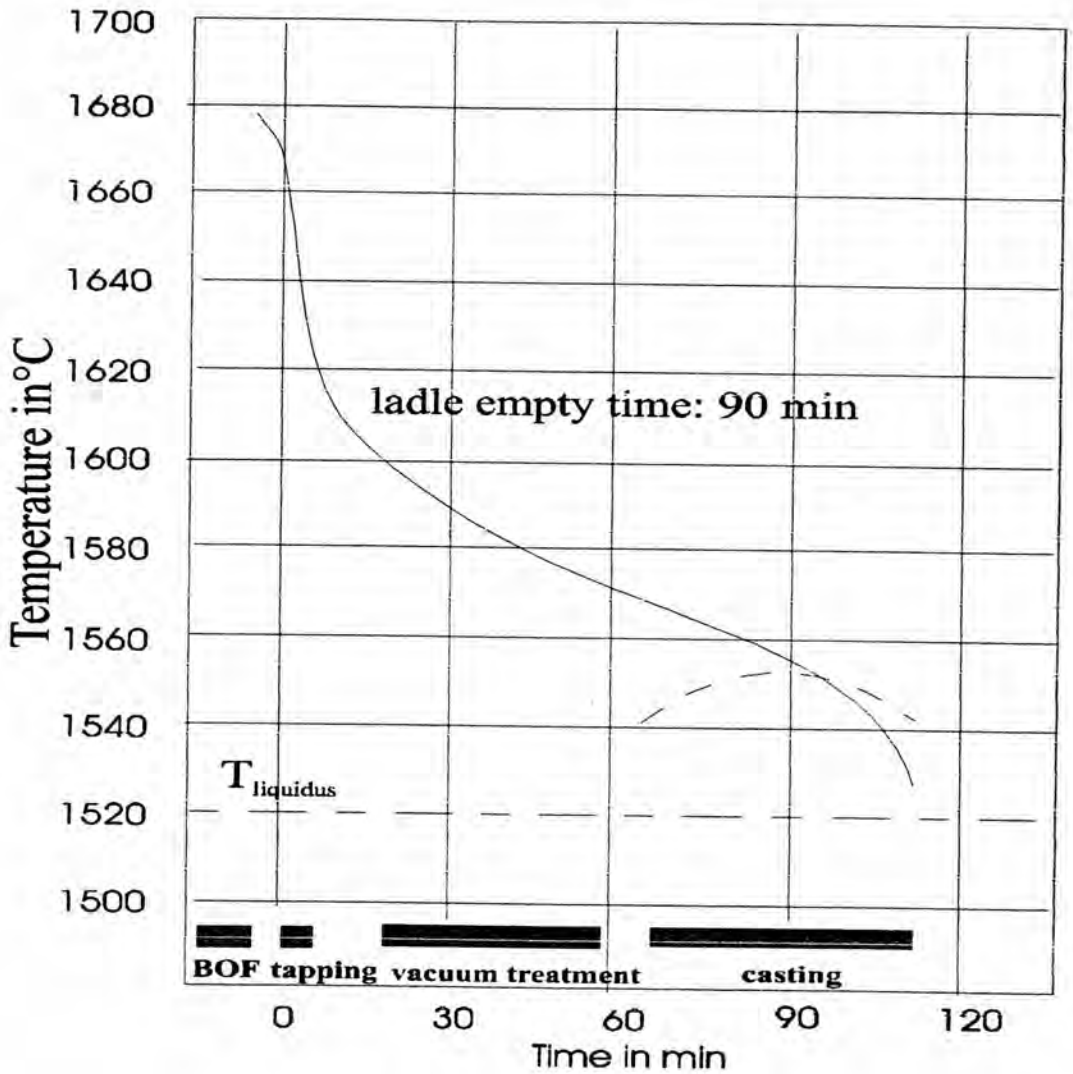

Figure 2.16 Example for temperature development of melt from the BOF to the tundish [53]